Published in final edited form as:
J Control Release. 2012 October 10; 163(1): 82–92. doi:10.1016/j.jconrel.2012.04.030.

Dual-Purpose Magnetic Micelles for MRI and Gene Delivery

Chunyan Wang[a,b], **Sowndharya Ravi**[a], **Gary.V. Martinez**[c], **Vignesh Chinnasamy**[a], **Payal Raulji**[a], **Mark Howell**[a], **Yvonne Davis**[a], **Mohindar S. Seehra**[d], and **Subhra Mohapatra**[a,b,*]

[a]Molecular Medicine Department, College of Medicine, University of South Florida, 12901 Bruce B. Downs Blvd., Tampa, FL, 33612, USA

[b]Nanomedicine Research Center, College of Medicine, University of South Florida, 12901 Bruce B. Downs Blvd., Tampa, FL, 33612, USA

[c]H.Lee Moffit Cancer Center and Research Institute, Tampa, FL, 33612, USA

[d]Department of Physics, West Virginia University, Morgantown, WV, 26506, USA

Abstract

Gene therapy is a promising therapeutic approach for treating disease, but the efficient delivery of genes to desired locations with minimal side effects remains a challenge. In addition to gene therapy, it is also highly desirable to provide sensitive imaging information in patients for disease diagnosis, screening and post-therapy monitoring. Here, we report on the development of dual-purpose chitosan and polyethyleneimine (PEI) coated magnetic micelles (CP-mag-micelles) that can deliver nucleic acid-based therapeutic agents and also provide magnetic resonance imaging (MRI). These 'theranostic' CP-mag-micelles are composed of monodisperse hydrophobic superparamagnetic iron oxide nanoparticles (SPIONs) loaded into the cores of micelles that are self-assembled from a block copolymer of poly (D, L-lactide) (PLA) and monomethoxy polyethylene glycol (mPEG). For efficient loading and protection of the nucleic acids the micelles were coated with cationic polymers, such as chitosan and PEI. The morphology and size distribution of the CP-mag-micelles were characterized and their potential for use as an MRI-probe was tested using an MRI scanner. The T2 relaxivity of micelles was similar to CP-mag-micelles confirming that coating with cationic polymers did not alter magnetism. Nanoparticles coated with chitosan:PEI at a weight ratio of 5:5 showed higher transfection efficiency in HEK293, 3T3 and PC3 cells than with weight ratios of 3:7 or 7:3. CP-mag-micelles are biocompatible, can be delivered to various organs and are safe. A single injection of CP-mag-micelles carrying reporter plasmids in vivo expressed genes for at least one week. Collectively, our results demonstrate that a structural reinforcement of SPIONs loaded in the core of an mPEG-PLA micelle coated with cationic polymers provides efficient DNA delivery and enhanced MRI potential, and affords a promising candidate for theranostics in the future.

Keywords

Chitosan and PEI coated magnetic micelles (CP-mag-micelles); magnetic resonance imaging (MRI); super paramagnetic iron oxide nanoparticles (SPIONs); gene delivery; theranostics

*Corresponding author. Tel.: 001-813-974-4127, Smohapa2@health.usf.edu.

1. Introduction

Gene therapy is used to treat hereditary diseases such as cystic fibrosis and also acquired diseases such as cancers [1], but is only as effective as its ability to deliver the therapeutic nucleic acid to a desired location. Vectors for gene delivery may be viral or nonviral. Viral vectors offer highly efficient gene transfer, but unwanted immune stimulation and the potential for mutagenesis have virtually eliminated them from clinical trials [2, 3]. In contrast, nonviral vectors are safe, have low immunogenicity, and are relatively inexpensive [4]. Examples of nonviral vectors include bacteria [5], cell-penetrating peptides [6], functionalized gold nanoparticles (NPs) or carbon nanotubes [7-10], and cationic polymers. Among these nonviral vectors, cationic polymers including polyethyleneimine (PEI) [11], poly(l-lysine) (PLL) [11, 12], chitosan [13], dendrimers [14, 15] and cationic lipids [16] have the advantages of being scalable for manufacturing in quantity, having low immunogenicity, the capacity for selective chemical modification and the ability to carry large inserts. Due to its superior transfection efficiency in a broad range of cell types, synthetic PEI has a privileged place among nonviral gene delivery systems. However, PEI is not degradable and the cytotoxicity increases with increasing molecular weight. Chitosan, which is obtained by deacetylation of chitin, is a biocompatible and biodegradable linear polymer whose cationic polyelectrolyte nature provides strong electrostatic interaction with negative charged DNA to form stable complexes that protect the DNA from degradation. However, the transfection efficiency of chitosan is very low and is dependent on its molecular weight, size and percentage of deacetylation [17]. The goal of a successful nonviral gene delivery system, therefore, is to achieve therapeutic efficacy while minimizing adverse effects of the delivery system on cells [18]. To develop such a safe and effective delivery vehicle, PEI-grafted chitosan, chitosan-grafted PEI or a chitosan-PEI composite have been tested and shown to have improved transfection efficiency and reduced toxicity compared to PEI alone [19-22].

For advanced gene delivery, it is desirable to monitor gene expression during or after therapy. Magnetic resonance imaging (MRI) is a powerful clinical imaging technique for diagnosis of a variety of diseases and post-therapy assessment. MRI contrast can be enhanced by the use of positive or negative contrast agents resulting in brighter (T_1-weighted) or darker (T_2-weighted) images, respectively. Superparamagnetic iron oxide NPs (SPIONs) are T_2 contrast agents that are widely used in molecular and cellular imaging applications [23, 24]. Recently, PEI- poly(ethylene glycol) (PEG)-chitosan coated SPIONs have been reported for DNA or siRNA delivery and MRI imaging [25, 26] and PEG-grafted PEI-complexed SPION for gene delivery and MRI imaging [27]. When incorporated into micelles, SPIONs have a longer half-life in circulation, improved biocompatibility, and show better contrast. SPION polymeric micelles were used successfully as MRI probes and for drug delivery [28-31].

Here, we report the development of a theranostic system consisting of dual-purpose magnetic micelles, CP-mag-micelles produced by coating SPION-loaded mPEG-PLA micelles with cationic polymers, such as chitosan and PEI. These mag-micelles were characterized by transmission electron microscopy (TEM), dynamic light scattering (DLS), Fourier transform infrared (FTIR) spectrometry and nuclear magnetic resonance (NMR). The potential of CP-mag-micelle for delivering DNA while maintaining superparamagnetic properties and biocompatibility, was tested through DNA binding assays, transfection studies in various cell lines, MR phantom imaging, biodistribution, in-vivo gene expression and WST assay.

2. Material and methods

2.1 Materials

Monomethoxy PEG (mPEG, Mw 2 kDa), branched PEI (Mw, 25kDa), 3,6-dimethyl-1,4-dioxane-2, 5-dione (DL-dilactide), stannous 2-ethylhexanoate, 1,2-dodecanediol, oleylamine and cyanoborohydride were purchased from Sigma. Iron (III) acetylacetonate ($Fe(acac)_3$), oleic acid, and benzyl ether were purchased from Acros Organics. Water-soluble chitosan (MW 10 kDa) was donated by Transgenex Nanobiotech Inc.

2.2 Synthesis of mPEG-PLA-OH

A series of mPEG-PLA-OH diblock copolymers were synthesized from DL-dilactide and mPEG of various molecular weights using stannous 2-ethyl-hexanoate as a catalyst by catalyzed ring-opening polymerization [32]. First, the DL-dilactide was dried with vacuum at room temperature for 4 hrs. The appropriate amount of mPEG was dried in a two-neck pre-dried round bottom flask with vacuum at 80°C for 3 hrs. Then certain amount of dry pure DL-dilactide, the stannous 2-ethyl-hexanoate (3% w/w) and 20 mL of toluene were added to two-neck flask and mixed with mPEG. The reaction solution was refluxed for 5 hrs in an oil bath (140°C) with argon gas protection. The product was precipitated with cold diethyl ether. The purified product was kept in vacuum at room temperature for 24 hrs. To determine the structure of the synthesized copolymers, FTIR spectra were performed using a NEXUS spectrometer. The block ratio and the chemical structure of mPEG-PLA were characterized by ^{1}H-NMR. The mPEG-PLA block compolymer was dissolved in $CDCl_3$ and ^{1}H-NMR spectrum was taken using a Bruker 250 spectrometer (Bruker, Rheinstetten, Gemany).

2.3 Preparation of CS-mag-micelles

SPIONs were prepared according to the procedure reported by Sun, et al [33]. The black SPION product was dissolved in dichloromethane in the presence of oleic acid (0.05 ml) and oleylamine (0.05 ml). The solvent evaporation method was used to prepare CS-mag-micelle by adding an SPION/mPEG-PLA dichloromethane solution dropwise to a chitosan solution with vigorous stirring. In a typical experiment, the mixture of 500 μl of 25 μg/μl mPEG-PLA in CH_2Cl_2 and 300 μl of 4 mg/ml SPION in CH_2Cl_2 solution was added dropwise to 10 ml of a 10 mg/ml solution of water-soluble chitosan with stirring. The organic solvent CH_2Cl_2 was allowed to evaporate slowly at ambient conditions overnight. The micelle solution was filtered through a nylon membrane filter (size cutoff 0.2 um) and freeze-dried. To prepare different weight ratios of chitosan-PEI-mag-micelles (also referred to as CP-mag-micelles)) (chitosan to PEI weight (wt) ratios, 7:3, 5:5, 3:7), different volumes of CS-mag-micelle solutions (2 mg/ml) were mixed with a PEI solution (2 mg/ml). The CP-mag-micelle solution was dialyzed with 5K molecular weight cutoff membrane to remove the free PEI. X-ray diffraction (XRD) measurements were acquired using a Rigaku D/Max diffractometer equipped with Cu-Kα radiation, λ=0.154185 nm. The magnetic data were taken with a vibrating sample magnetometer (Model 4500 by EG&G/Princeton Applied Research Corp) at room temperature.

2.4 Plasmid preparation

The plasmid pCMV-tdTomato (Clontech) encoding the tdTomato red-fluorescent protein was grown in XL1-Blue cells and purified by MaxiPrep plasmid purification kit (Invitrogen Corporation, Carlsbad, CA). The pRL renilla luciferase plasmid (Promega Corporation, Madison, IL) and pSV40 luciferase were grown in E. coli XL10. The DNA concentration and purity were determined prior to using in transfection assays.

2.5 Preparation of CP-mag-micelle:DNA complexes

The CP-mag-micelles (0.2 μg/μl, 10 kD) and a plasmid DNA solution (0.2 μg/μl) in PBS were prepared separately. The plasmid DNA solution was added drop-wise to CP-mag-micelles solution and vortexed for 20 minutes.

2.6 MR phantom imaging

Various dilutions of mag-micelles, CP-mag-micelles (wt ratio, 5:5), CP-mag-micelles:DNA (wt ratio of chitosan:PEI:DNA, 5:5:1) were diluted with deionized water. The concentrations of iron in the micelles were determined according to a protocol reported by Mykhaylyk [34]. 200 μl aliquots of various micelle solutions were added to a 96 well plate. MR images were obtained using an Agilent ASR 310 7 Tesla MRI high-field scanner. Multi-echo transverse relaxation experiments (MEMS) were performed in imaging mode to determine measure T_2 values. Nonlinear least square fitting was performed in MATLAB (Mathworks, Inc) on a pixel-by-pixel basis. A region of interest (ROI) was drawn for each well, where the mean value was used to determine the transverse molar relaxivity r_2. The image was recorded with Vnmrj 3.0.

2.7 Gel retardation assay

The CP-mag-micelles:DNA complexes were mixed with a loading buffer and loaded onto a 0.8% agarose gel containing ethidium bromide. Gels were electrophoresed at room temperature in Tris/Borate/EDTA buffer at 80 V for 60 min. DNA bands were visualized using a Chemi DOX TM XRS imaging system (Bio-RAD, CA, USA).

2.8 Measurement of particle sizes

The hydrodynamic particle sizes of the mag-micelles, CP-mag-micelles and CP-mag-micelles:DNA complex in DMEM cell culture media were measured at 25°C using a DynaPro DLS plate reader (Wyatt Technology, Germany). The morphology of the SPIONs and multi-layered mag-micelles was determined by TEM.

2.9 Cytotoxicity test

In vitro cytotoxicity was evaluated in PC3 cells using the WST-1 colorimetric assay with 2-(4-iodophenyl)-3-(4-nitrophenyl)-5-(2, 4-disulfophenyl)-2H-tetrazolium monosodium salt reagent. PC3 cells were seeded in a 96-well plate using standard DMEM supplemented with 10% fetal bovine serum and 1 % penicillin G and streptomycin. Various concentrations of NPs were added to the well in triplicate. The cells were cultured for 72 hrs in an incubator at 37°C under 5% CO_2. After 68 hrs, 10 μL of WST-1 (diluted 1:4 with phosphate buffer) was added and cells were incubated for an additional 4 hrs. Cell viability was measured at 450 nm in a microplate reader (Synergy H4 Hybrid reader, Biotek). Cell viability (%) was calculated according to the following equation: Cell Viability (%) = $100\times(OD_{sample}/OD_{control})$

2.10 In vitro transfection of HEK 293 cells, PC3 cells and 3T3 cells with CP-mag-micelle: DNA complexes

Cells were seeded 24 hrs prior to transfection into a 96-well plate at a density of 5000 cells per well in 100 μl of complete medium (DMEM containing 10% FBS, supplemented with 2 mM l-glutamate, 50 U/ml penicillin and 50 μg/ml streptomycin). At the time of transfection, the medium in each well was replaced with 500 μl of fresh complete medium. An amount of NPs equivalent to 0.2 μg of DNA was added to each well. The plate was placed on a magnet for 30 mins and then incubated for 48 hrs. Transfection with lipofectamine-DNA (LipofectamineTM, LTX, Invitrogen) complexes was performed as positive controls

according to the manufacture's protocol. All transfection experiments were performed in triplicate.

2.11 Transfection efficiency using luminometric assay for luciferase

For luminometric assay, the cells were plated in 12-well plate at a density of 105 cells per well in 1 ml of complete medium. After 48 hrs incubation with plasmid (tomatoDNA: pRL-Luciferase:SV40-luciferase (wt ratio, 10:1:1)) complexed nanovectors, cells were collected with 50 μl of 1× cell-passive buffer (Promega). The luciferase activity in cell extracts was measured using a dual luciferase assay kit (Promega) on a luminometer. The light units (LU) were normalized against protein concentration in the cell extracts, which was measured using a BCA protein assay kit (ThermoScientific). Luciferase activity in cell lysates was expressed as relative light units (LU/min per μg of protein in the cell lysate).

2.12 TEM imaging of cell ultra-sections

PC3 or HEK 293 cells were incubated with CP-mag-micelle:DNA complex (wt ratio of chitosan:PEI:DNA, 5:5:1) for 24 hrs. The cells were trypsinized and immediately prefixed in 1% paraformaldehyde and 0.5% glutaraldehyde buffered with 0.5% sodium cacodylate (pH 7.1) for 10 min at 4°C, then pelleted by centrifugation at 1200 rpm for 5 min. The cell pellets were fixed in 2% paraformaldhyde-2.5% glutaraldehyde-0.05% sodium cacodylate, pH 7.1 for 30 min at 4 °C. After centrifugation, the pellets were collected and washed with 0.2 M sodium cacodylate, pH 7.4. Osmium tetroxide (1%) in sodium cacodylate buffer was then used for 1 hr for post-fixation at room temperature, followed by three washings in deionized water. Dehydration of cell pellets was then performed in an ascending series of ethanol concentrations--10%, 35%, 50%, 70%, 95% and 100% ethanol--for ten minutes each, followed by 100% acetone dehydration for 10 minutes. The pellets were then infiltrated with Embed 812 epoxy resin (Electron Microscopy Science, Fort Washington, PA) in a stepwise manner with ratios of acetone to Embed of 3:1, 1:1, 1:3 for 30 min each. Finally, the pellets were transferred into pure resin for 24 hrs, and allowed to harden at 40°C and 60 °C for 24 hrs respectively. Ultrathin sections were cut with a Leica ultramicrotome and imaged with a JEOL 1200 EX transmission electron microscope, operating at an accelerating voltage of 80 kV. The cell uptake of CP-mag-micelles was also visualized with fluorescent-labeled micelles, which were prepared by reacting Cy5.5-NHS with CP-mag-micelle (wt ratio 5:5) overnight. The Cy 5.5-CP-mag-micelles were purified by dialysis in a dialysis membrane with molecular weight cutoff of 1K until no free Cy5.5 was detectable in the dialysis solution by spectrophotometric measurement at 650 nm. Three hours after Cy5.5-CP-mag-micelles were incubated with HEK293 cells, the cells were fixed and stained with DAPI. The distribution of NPs inside the cells was imaged with the multiphoton Olympus BX61W1 confocal microscope.

2.13 In vivo tissue distribution of fluor-labeled CP-mag-micelles

To monitor the biodistribution of CP-mag-micelle after i.p. and i.v. administration, 500 μl of Cy5.5-CP-mag-micelle solution containing 500 μg CP-mag-micelle and 6.25 μg Cy5.5 was administered i.p or i.v. to C57BL/6 mice (6-8 week old). After 4 hrs, the mice were euthanized via CO2 asphyxiation. The organs were removed, weighted and scanned for fluorescence using the Xenogen IVIS imager (Caliper Life Sciences Inc, MA, USA).

2.14 *In vivo* gene delivery and clearance test of CP-mag-micelle:DNA complexes

500 μl of CP-mag-micelle:DNA (wt ratio of chitosan:PEI:DNA, 5:5:1) containing 20 μg DNA or 500 μl PBS was administered i.p. to C57BL/6 mice (6-8 week old). After 1, 2 and 7 days, the mice were euthanized via CO2 asphyxiation and liver, spleen, kidney, lung and

prostate were removed and fixed in 10% formalin for hematoxylin and eosin (H&E) staining.

A part of the same organs was embedded in OCT freezing medium and kept at -80°C until needed. The frozen tissues were sliced in 5 μm thick sections, fixed in 4% paraformaldehyde and stained using Prussian blue to indicate the presence of iron. For analysis of DNA expression, the 5 μm frozen sections were fixed with 4% paraformaldehyde and immunostained with anti-red fluorescent protein (RFP) and DAPI (nuclear DNA stain) (Vector Lab). All images were made using an Olympus BX51 microscope equipped with a DP-72 high-resolution digital camera (Olympus Imaging America Inc., Center Valley, PA).

2.15 Statistical analysis

Data are expressed as mean plus or minus standard deviation. Statistical analysis was performed using the unpaired Student's t-test. Differences were considered statistically significant for $p < 0.05$.

3. Results and Discussion

3.1 Preparation and characterization of multilayered mag-micelles

The polymeric micelle has been widely studied as a novel nanomedicine platform for anticancer drug delivery and diagnostic imaging applications over the past decade [29-31, 35-37]. This nanoplatform was expected to prolong the drug circulation time in blood while reducing direct contact between drugs and healthy tissues or organs. It was also reported that clustering of the MRI contrast agent SPION inside the micelle core resulted in high T_2 relaxivity (>400 Fe mM^{-1} s^{-1}) [30]. In this study, we developed a nanovector based on the polymeric micelles for DNA delivery. The assembly of the nanovector is shown in Figure 1. The hydrophobic SPIONs were synthesized according to the procedures of Sun et al [33]. The XRD spectra confirmed the formation of Fe_3O_4 (Figure 2A) [38, 39]. The particle size determined from the Scherrer Broadening of the XRD lines is 7.0 ± 0.6 nm. TEM images (Figure 2C) showed an average size of 6 nm in agreement with the XRD results. The magnetic properties of the SPION powder at 300K analyzed using a vibrating sample magnetometer show no hysteresis (Figure 2B) characteristic of superparamagnetism with saturation magnetism $M_s \cong 23$ emu/g. This magnitude of M_s is consistent with that reported for similarly prepared 6 nm Fe_3O_4 NPs with a blocking temperature of about 20K [39] .

The synthesized SPIONs which were coated with hydrophobic chains from oleic acid and oleylamine self-assembled to needle shape as shown in figure S1. To increase sensitivity of MRI, hydrophobic SPIONs were loaded into the core of micelles (referred to as mag-micelles) self-assembled from an amphiphilic block copolymer of mPEG- poly (D, L-lactide) (PLA). The block copolymer mPEG-PLA was synthesized by a ring opening polymerization of D, L-lactic acid using monomethoxy-terminated PEG (2KD) as a macro-initiator and $S_n(Oct)_2$ as catalyst. The block copolymer was characterized by FTIR and NMR. Figure 3A shows the FTIR of mPEG and mPEG-PLA. The strong absorption at 1760 cm^{-1} is assigned to – C = O stretch of PLA, while the band at 1087 and 1184 cm^{-1} is due to C-O-C stretch of PEG and PLA, respectively. The ^{1}H-NMR was obtained to further confirm that PLA was copolymerized with mPEG as shown in Figure 3B. The integral of the signal at 3.3 ppm, which is attributed to the three equivalent hydrogen atoms of the methyl group on mPEG-OH was used as the internal standard. The molecular weight of the PLA block in the copolymer was calculated to be 13 kDa using an internal standard. The diameter of formed mag-micelles spheres ranged from 35 to 50 nm as shown in figure 2D.

To ensure biocompatibility and stability *in vivo* and proper intracellular trafficking, the mag-micelles were coated with the cationic polymers, chitosan and PEI. First, the chitosan coated mag-micelles (CS-mag-micelles) were prepared by solvent evaporation. Second, PEI was added to CS-mag-micelles at different weight (wt) ratios to form chitosan-PEI coated mag-micelles (CP-mag-micelle). A 50 kDa molecular weight-cutoff dialysis bag was used to remove uncoated PEI, and DLS was used to measure the distribution of the size and the peak of the hydrodynamic radius of different layers of mag-micelles in aqueous solutions (Figure S2). The average hydrodynamic radius of CS-mag-micelles is 49.8 nm (Figure S2B), which is larger than that of mag-micelles (22.7 nm). When PEI was added to the coating of CS-mag-micelles, the average radius of CP-mag-micelles was further increased. CP-mag-micelles with different wt ratios of chitosan:PEI, 7:3, 5:5 and 3:7, formed particles with average radii of 65.2 nm, 53.8 nm, and 61.3 nm, respectively.

The morphology of mag-micelles and CP-mag-micelles was determined by TEM. Figure 2D and 2E show well-defined core/shell structures of mag-micelles with a high density of SPION clusters inside the micelles. The size of the CP-mag-micelles was 50-70 nm, which is somewhat larger than the mag-micelles (35-40 nm).

The Tomato-DNA plasmids were bound to the surface of CP-mag-micelles by electrostatic forces. As shown in the TEM images (Figure 2F), the surface of the CP-mag-micelles was encircled by DNA plasmids. The size distribution of the CP-mag-micelle:DNA complex is shown in Figure S2. The average hydrodynamic radius of the CP-mag-micelle:DNA complex increased with PEI concentration on the coatings from 107.1 nm with chitosan:PEI:DNA at a wt ratio of 7:3:1 to 132.1 nm with a chitosan:PEI:DNA wt ratio of 3:7:1.

The formation of the multilayered mag-micelles was further confirmed by FTIR.Figure S3A shows the FTIR bands characteristic of oleic acid-coated hydrophobic SPION. The bands at 574 and 424 cm^{-1} were due to Fe-O vibration bands. Surface bonded oleic acid can be observed by the presence of 2911 and 2846 cm^{-1} assigned to C-H stretch, and 1461 cm^{-1} (C-H bending). In the FTIR of mag-micelles (Figure S3B), absorption peaks due to mPEG-PLA (e.g., 1037 and 1139 cm^{-1} peaks from PEG C-O-C and PLA, and1749 cm^{-1} peak from C=O stretching bands respectively) were observed. In addition, 3200-3600 cm^{-1} broad band from O-H stretching was also observed. In the FTIR of CS-mag-micelles (Figure S3C) and CP-mag-micelles (Figure S3D) more broad bands at 3200-3600 cm^{-1} due to N-H and O-H stretching were observed. Bands at 1508 cm^{-1} and 1641cm^{-1} were observed from the N-H bend of amide and amine respectively. These observations confirmed that CS and PEI were coated on the surface of mag-micelles. The mechanism of CS and PEI coating onto the surface of the mag-micelle might be due to the electrostatic force. The zeta potential of mag-micelle is -16.70 mV. When mag-micelles are bound with positively-charged chitosan to form CS-mag-micelles, the zeta potential of CS-mag micelles was changed to +6.58 mV. When PEI was added to the CS-mag-micelles, the zeta potential of CP-mag-micelles was further increased to +17.89 mV. The increase in zeta potential confirmed coating of mag-micelles with chitosan and PEI.

3.2 Complexes of CP-mag-micelles and DNA

The ability of the vector to form complexes with nucleic acids is a fundamental requirement for gene delivery. The condensation capability of different layers of mag-micelles with DNA was evaluated using agarose gel electrophoresis as shown in Figure 4. In this assay, DNA which was bound to the mag-micelles remained in the loading wells, while unbound DNA migrated down the agarose gel. It was observed that CS-mag-micelles could not completely retarded DNA until the chitosan:DNA wt ratio reached 10:1. However, the migration of DNA was retarded completely with CP-mag-micelles irrespective of chitosan:PEI wt ratios.

These results suggest that PEI enhanced DNA binding to mag-micelles. During transfection it is critical to protect DNA from degradation by nucleases and destructive enzymes within lysosomes, which can reduce transfection efficiencies. We examined whether the addition of PEI to CS-mag-micelles could improve binding capacity and protection of DNA. The gel retardation analysis provided information about DNA protection by the mag-micelles. Figure 4 shows that DNA bound by CS-mag-micelles at a wt ratio of 5:1 or 10:1 was not protected as evidenced by ethidium bromide staining in the loading wells. On the other hand, PEI and CP-mag-micelles fully protected bound DNA from staining, as seen by a lack of visualized DNA in the wells. These results are in concordance with published reports [25].

3.3 Cell transfection assay

Gene therapy can be performed both ex vivo and in vivo. In the ex vivo method, the plasmid DNA is first introduced into cells, the cells are allowed to grow and divide for a few days and then the cells carrying plasmid DNA are injected into the patient. In the in vivo method, the plasmid DNA is delivered directly into the patient's body. We tested the ability of CP-mag-micelles to deliver plasmid DNA to various cultured cells in vitro using plasmid DNA encoding Tomato protein (pCMVtdTomato) as a reporter (with excitation and emission maxima of 554 and 581 nm, respectively). To visualize the gene delivery efficacy, cells were plated in 96-well plates overnight and then incubated with various transfection agents 2 μg/ml DNA. A magnet was placed under the plate for half hour to enhance the transfection. The magnet was removed and the cells were incubated for 48 hours. The fluorescent images in figure 5 (A, B) show that nanocomplexes of PEI:DNA (wt ratio, 10:1) and chitosan-PEI coated mag-micelles (CP-mag-micelles) irrespective of chitosan:PEI wt ratios, readily delivered tomato DNA in HEK293 and 3T3 cells. Consistent with gel retardation data, chitosan-DNA nanocomplexes, even at higher wt ratios (chitosan:DNA, 10:1) did not transfect cells. Similar results were obtained when PC3 cells were transfected with various CP-mag-micelles (Figure S4). Cells receiving no treatment were also imaged for reference. These results demonstrate the ability of CP-mag-micelles to deliver DNA into the cells and produce expression levels similar to those commercially available transfection agents, such as lipofectamine.

Transfection efficiency was quantified using Renilla luciferase reporter plasmids (pRE-luc). HEK293 cells were transfected with nanocomplexes consisting of various combinations of CP-mag-micelles and pRE-luc. Results shown in Figure 6A suggest that in HEK 293 cells, nanocomplexes of CP-mag-micelle with DNA induce luciferase activity similar to lipofectamine-DNA complex, and higher than with PEI-DNA complexes. The transfection efficiency of CP-mag-micelles as a function of DNA dose was also evaluated. At 0.5 μg DNA/ml, the transfection efficiency of all three CP-mag-micelle:DNA complexes, with chitosan:PEI:DNA wt ratios, 7:3:1, 5:5:1 or 3:7:1 is comparable to that of PEI-DNA complexes. When the dose of DNA was further increased from 1 to 2 μg DNA/ml, the transfection efficiencies of CP-mag-micelles were much higher than PEI and were comparable to lipofectamine.

We examined the potential of CP-mag-micelles to deliver DNA to 3T3 cells, since these cells are resistant to transfection with chitosan-DNA NPs [40].) At low DNA concentrations (0.5 μg DNA/ml), the transfection efficiency of CP-mag-micelle and PEI for 3T3 cells was lower than with Lipofectamine (Figure 6B). When the DNA concentration was increased to 1 μg/ml, the transfection efficiency of CP-mag-micelle increased with an increase in PEI wt ratio. The transfection efficiency of CP-mag-micelle:DNA (with chitosan:PEI:DNA wt ratio, 3:7:1) was higher than Lipofectamine, but significantly lower than PEI:DNA (10:1). However, at 2 μg DNA/ml, the cell transfection efficiency of all three CP-mag-micelles increased significantly compared to Lipofectamine. The transfection efficiency of CP-mag-

micelle:DNA (wt ratios of chitosan:PEI:DNA, 5:5:1 and 7:3:1) was 10-fold more than Lipofectamine and PEI:DNA (10:1). These results demonstrate that nanocomplexes of CP-mag-micelles can transfect 3T3 cells with high efficiency compared to Lipofectamine or PEI.

We next examined the transfection efficiency of CP-mag-micelles in the difficult-to-transfect cancer cell line, PC3. As shown in Figure 6C, the transfection efficiency CP-mag-micelles in PC3 cells depended on the dose of DNA irrespective of the PEI wt ratio. At 1 or 2 μg DNA/ml, CP-mag-micelle:DNA (with chitosan:PEI:DNA wt ratio, 7:3:1) showed the highest cell transfection efficiency, which weas significantly higher than Lipofectamine. The highest transfection efficicency was seen with CP-mag-micelle:DNA (wt ratio of chitosan:PEI:DNA, 5:5:1) complexed with 3 μg/ml DNA. From these results it can be concluded that the synergistic effect of chitosan and PEI endowed CP-mag-micelles with the ability to produce a greater transfection efficiency than PEI itself and one that is comparable to or better than Lipofectamine depending on the dose and cell line.

The degree of synergy between chitosan and PEI depends on the structure of the NPs and the type of cell line, as reported [21, 41]. The ability of chitosan/PEI to transfect cells better than chitosan alone can be attributed to the higher amine content in the complex and the PEI's proton sponge effect that facilitates the escape of DNA from endosomes. The transfection efficiency of chitosan/PEI is higher than that of PEI alone due in part to the weaker condensation ability of the complex, which would result in an easier release of DNA from the complexes inside the cells [42].

3.4 Cell viability test

To determine the cytotoxicity of CP-mag-micelles, cell viability was measured by WST assay. PC3 and HEK293 cells were incubated in the presence of different combinations of CP-mag-micelles for 72 hrs. Cells without NPs were used as a positive control with a cell viability of 100%. The results in Figure 7 show that CS-mag-micelles and CP-mag-micelles show some dose-dependent cytotoxicity but lower than PEI. The CP-mag-micelles with chitosan:PEI wt ratios of 7:3 and 5:5 did not show any cytotoxicity even at the high concentration of 80 μg/ml in PC3 cells. However, CP-mag-micelles with chitosan:PEI at a wt ratio, 3:7 showed a dose-dependent increase in cytotoxicity . These results indicated that CP-mag-micelles with chitosan:PEI wt ratios of 7:3 and 5:5 are ideal for delivering genes with no toxicity. Since CP-mag-micelleCP-mag-micelle with chitosan:PEI wt ratio, 5:5 demonstrated high transfection efficiency without cytotoxicity, it was chosen for further studies.

3.5 Cell uptake mechanism

NPs can be internalized either by receptor-mediated endocytosis or by macropinocytosis, caveolae-mediated endocytosis or lipid raft-mediated endocytosis on cell membranes via hydrophobic or electrostatic interactions [43]. In order to determine the mechanism of cellular uptake and intracellular distribution of CP-mag-micelle:DNA nanocomplexes, PC3 cells were transfected with NPs for 24 hrs, then trypsinized, fixed and analyzed by TEM. As shown in Figure 8(a), NPs attached to the plasma membrane (Figure 8(a)A) were endocytosed by macropinocytosis (Figure 8(a)D) or lipid raft-mediated endocytosis (Figure 8(a)E). The NPs were present inside endosomes in the cytoplasm as shown in Figure 8(a). After endocytosis, the NPs in endosomes can move into the cytoplasm by the aid of PEI [44], which absorbs the protons produced during the acidification process in the mature endosome. In order to maintain electric neutrality, a parallel influx of Cl^{-1} ions and water accompanies the influx of protons. This process can induce swelling and eventual rupture of the endosome membrane allowing its contents to escape. Figure 8(a) H shows the rupture of

the membrane of the endosome and escape of NPs moving toward the nuclear membrane. Some particles pass through the nuclear membrane via nuclear pores and enter the nucleus as shown in Figure 8(a) B, F, G . Further, some NPs were taken up by the liposome as shown in Figure 8(a) C. Similar results were observed in HEK 293 cells as shown in figure S5.

To better visualize the escape of NPs from endosomes, the CP-mag-micelles were complexed with Cy5.5, a near-infrared imaging dye to track the NPs after transfection. HEK293 cells were transfected with Cy5.5 complexed with CP-mag-micelle (chitosan:PEI wt ratio, 5:5) for 3 hours, nuclei were stained blue with the DNA-staining agent, DAPI, and the distribution of NPs inside the HEK 293 cells was examined by confocal fluorescent microscopy (Figure 8(b)). Results showed the CP-mag-micelles distributed throughout the cells, which indicated that endosomes were being disrupted and releasing the Cy5.5- CP-mag-micelles into the cytoplasm. Furthermore, some NPs were observed in the nucleus.

3.6 *In vitro* MRI

In addition to delivering the gene-expressing plasmid, the CP-mag-micelles were also designed to act as an MRI contrast agent to allow monitoring of the outcome of gene therapy. To determine whether CP-mag-micelles retained sufficient magnetism to be detectable by MRI, mag-micelles, CP-mag-micelles and CP-mag-micelles:DNA complexes with chitosan:PEI wt ratio, 5:5 were analyzed by MR phantom imaging. Figure 9A and 9B show the visual and quantitative contrast respectively, provided with various Fe concentrations. The r_2 relaxitivity of mag-micelles (162.9 $mM^{-1}S^{-1}$) were similar to CP-mag-micelles (141.7 $mM^{-1}S^{-1}$) and CP-mag-micelles:DNA (111.7 $mM^{-1}S^{-1}$) confirming that coating with cationic polymers did not alter magnetism significantly. These relaxitivity r_2 values were significantly larger than those for SPION-dextran NPs (30-50 Fe $mM^{-1}S^{-1}$) [45] and Fe_3O_4-PEG-PAE (poly(b-amino ester) micelle (92.7mM^{-1} s^{-1}[46]). These r_2 values were also comparable to the values of reported SPION micelles:110.4 for folate-free SPION-DOX-micelles [31], 121.2 for PEG4.3k–PCL7.2k–SPION [36], 207.99 Pluoronic-F127-SPION micelles [37].

3.7 Biodistribution and clearance of CP-mag-micelles *in vivo*

Iron oxide NPs coated with PEI-PEG-chitosan are considered safe for gene delivery [25]. However, CP-mag-micelles differ from the above particles by having (i) SPIONs in the core of the PEG-PLA micelles, which is expected to increase the plasma/tissue half-life of these particles, (ii) a modified composition of chitosan and PEI in the polymeric layer, and (iii) a novel method of preparation. These modifications necessitated determinations of the biodistribution, clearance and safety of CP-mag-micelles.

For biodistribution studies, mice were injected with 500 μl of 1 mg/ml Cy5.5-CP-mag-micelles by i.p or i.v. Four hours after administration, lungs, liver, kidney, spleen and prostate tissues were excised and scanned for Cy5.5 expression using the IVIS-100 imaging system, as shown in Figure 10A. The average Cy5.5 intensity of different organs obtained by photon emissions divided by the weight of organs was shown in figure 10B. Tissue binding was higher in spleen, liver and kidney than other tissues. Moreover, i.v. administration showed better tissue accumulation of NPs in all organs than i.p. administration, with the exception of the prostate tissue.

The in vivo clearance of CP-mag-micelles was determined by Prussian blue staining accompanied with H&E staining of fixed paraffin tissue sections 1, 2 and 7 days after i.p. administration of CP-mag-micelle:DNA nanocomplexes (wt ratio of chitosan:PEI:DNA, 5:5:1) in mice (n = 6). Figure 11(a) shows the H&E staining of liver 1, 2 and 7 days after i.p.

administration. At the same time, Prussian blue staining was used to determine accumulation of iron particles inside the organs. Despite relatively high levels of NP accumulation in liver, spleen, lung and prostate, which were confirmed by the presence of iron, no morphological alterations in the histology of the organs were observed. Overall, this study indicates that the CP-mag-micelles were well tolerated in mice and could be cleared by the body in 7 days.

The intracellular SPIONs get degraded by hydrolytic enzymes in lysosomes through low pH exposure, and iron ions are incorporated into the hemoglobin pool [47, 48]. We examined whether SPIONs were degraded following treatment with CP-mag-micelles:DNA complexes. Liver sections were stained with Prussian blue for iron detection. As shown in figure 11(a), positive Prussian blue staining was observed one day after i.p injection, which gradually decreased from day 2 to day 7. Very little Prussian blue staining was observed at day 7, indicating nearly complete degradation of SPIONs. These studies demonstrate that CP-mag-micelles are biocompatible and nontoxic, and can be cleared from tissues within one week.

3.8 Gene transfection efficiency of CP-mag-micelles in vivo

To evaluate the potential of CP-mag-micelles to deliver genes in vivo, CP-mag-micelles:DNA (wt ratio of chitosan:PEI:DNA, 5:5:1) were administrated i.p. to male mice (n = 6). After 1, 2 and 7 days, the mice receiving CP-mag-micelle:DNA or PBS (control) were euthanized and the organs were collected. Red-fluorescent protein (Tomato) expression in the liver and prostate was observed by staining the frozen sections with anti-RFP and DAPI, as shown in Fig. 11(b). The CP-mag-micelles were able to deliver DNA as evidenced by the high tomato protein expression in the liver and prostate tissues of NP-treated mice. It is evident that gene expression started as early as day 1, increased on day 2, and continued up to day 7. Furthermore, the gene expression was not restricted to the edge of the tissue, but was seen distributed inside the organs.

4. Conclusions

The core shell-structured CP-mag-micelles reported here have high MRI relaxivity and can efficiently transfect various cell lines, such as HEK 293, 3T3 and PC3 cells in vitro. These particles can deliver genes with higher transfection efficiency than Lipofectamine or PEI, in part due to the synergistic effect of chitosan and PEI cationic polymer coatings. TEM and confocal images show that endocytosis is the likely mechanism of cellular uptake and that the NPs are released by endosome escape inside PC3 and HEK 293 cells. The cell viability studies demonstrated that CP-mag-micelles with chitosan to PEI wt ratios of 7:3 and 5:5 are nontoxic to cells. The biodistribution experiments in mice showed that most CP-mag-micelles accumulate in the liver, lung, spleen and prostate. The in-vivo clearance studies of CP-mag-micelles further demonstrated that these particles are biocompatible and safe. Furthermore, these NPs were able to deliver genes efficiently into mice, which persisted for at least 7 days. Collectively, these results suggest that CP-mag-micelles are a promising vehicle for gene delivery and for MRI monitoring both ex-vivo and in-vivo.

supplementary Material

Refer to Web version on PubMed Central for supplementary material.

Acknowledgments

This work is supported by 1R41CA139785 and 5R01CA152005 grants from National Institute of Health awarded to SM. We would like to thank Dr. Gary Hellermann for critical reading of the manuscript. We also acknowledge the assistance of the Lisa Muma Weitz Laboratory for Advanced Microscopy and Cell Imaging and the Mason Laboratory for Small Animal Imaging at USF Health and the MRI facility at the H. Lee Moffitt Cancer Center.

References

1. Conese M, Ascenzioni F, Boyd AC, Coutelle C, De Fino I, de Smedt S, Rejman J, Rosenecker J, Schindelhauer D, Scholte BJ. Gene and cell therapy for cystic fibrosis: From bench to bedside. Journal of Cystic Fibrosis. 2011; 10:S114–S128. [PubMed: 21658631]
2. Edelstein ML, Abedi MR, Wixon J. Gene therapy clinical trials worldwide to 2007 - an update. Journal of Gene Medicine. 2007; 9:833–842. [PubMed: 17721874]
3. Thomas CE, Ehrhardt A, Kay MA. Progress and problems with the use of viral vectors for gene therapy. Nature Reviews Genetics. 2003; 4:346–358.
4. Guo JF, Bourre L, Soden DM, O'Sullivan GC, O'Driscoll C. Can non-viral technologies knockdown the barriers to siRNA delivery and achieve the next generation of cancer therapeutics? Biotechnology Advances. 2011; 29:402–417. [PubMed: 21435387]
5. Chang CH, Cheng WJ, Chen SY, Kao MC, Chiang CJ, Chao YP. Engineering of Escherichia coli for Targeted Delivery of Transgenes to HER2/neu-Positive Tumor Cells. Biotechnology and Bioengineering. 2011; 108
6. Chen YA, Kuo HC, Chen YM, Huang SY, Liu YR, Lin SC, Yang HL, Chen TY. A gene delivery system based on the N-terminal domain of human topoisomerase I. Biomaterials. 2011; 32:4174–4184. [PubMed: 21406310]
7. McIntosh CM, Esposito EA, Boal AK, Simard JM, Martin CT, Rotello VM. Inhibition of DNA transcription using cationic mixed monolayer protected gold clusters. Journal of the American Chemical Society. 2001; 123:7626–7629. [PubMed: 11480984]
8. Han G, Martin CT, Rotello VM. Stability of gold nanoparticle-bound DNA toward biological, physical, and chemical agents. Chemical Biology & Drug Design. 2006; 67:78–82. [PubMed: 16492152]
9. Han G, Chari NS, Verma A, Hong R, Martin CT, Rotello VM. Controlled recovery of the transcription of nanoparticle-bound DNA by intracellular concentrations of glutathione. Bioconjugate Chemistry. 2005; 16:1356–1359. [PubMed: 16287230]
10. Gao LZ, Nie L, Wang TH, Qin YJ, Guo ZX, Yang DL, Yan XY. Carbon nanotube delivery of the GFP gene into mammalian cells. Chembiochem. 2006; 7:239–242. [PubMed: 16370018]
11. Lungwitz U, Breunig M, Blunk T, Gopferich A. Polyethylenimine-based non-viral gene delivery systems. European Journal of Pharmaceutics and Biopharmaceutics. 2005; 60:247–266. [PubMed: 15939236]
12. Kaneshiro TL, Wang X, Lu ZR. Synthesis, characterization, and gene delivery of Poly-L-lySine octa(3-aminopropyl)silsesquioxane dendrimers: nanoglobular drug carriers with precisely defined molecular Architectures. Molecular Pharmaceutics. 2007; 4:759–768. [PubMed: 17705440]
13. Corsi K, Chellat F, Yahia L, Fernandes JC. Mesenchymal stem cells, MG63 and HEK293 transfection using chitosan-DNA nanoparticles. Biomaterials. 2003; 24:1255–1264. [PubMed: 12527266]
14. Dennig J. Gene transfer in eukaryotic cells using activated dendrimers, Dendrimers V: Functional and Hyperbranched Building Blocks. Photophysical Properties, Applications in Materials and Life Sciences. 2003; 228:227–236.
15. Wu HM, Pan SR, Chen MW, Wu Y, Wang C, Wen YT, Zeng X, Wu CB. A serum-resistant polyamidoamine-based polypeptide dendrimer for gene transfection. Biomaterials. 2011; 32:1619–1634. [PubMed: 20951425]
16. Morille M, Passiran C, Vonarbourg A, Clavreul A, Benoit JP. Benoit, Progress in developing cationic vectors for non-viral systemic gene therapy against cancer. Biomaterials. 2008; 29:3477–3496. [PubMed: 18499247]
17. Jiang HL, Kim YK, Arote R, Nah JW, Cho MH, Choi YJ, Akaike T, Cho CS. Chitosan-graft-polyethylenimine as a gene carrier. Journal of Controlled Release. 2007; 117:273–280. [PubMed: 17166614]
18. Breunig M, Lungwitz U, Liebl R, Goepferich A. Breaking up the correlation between efficacy and toxicity for nonviral gene delivery. Proceedings of the National Academy of Sciences of the United States of America. 2007; 104:14454–14459. [PubMed: 17726101]

19. Lou YL, Peng YS, Chen BH, Wang LF, Leong KW. Poly(ethylene imine)-g-chitosan using EX-810 as a spacer for nonviral gene delivery vectors. Journal of Biomedical Materials Research Part A. 2009; 88A:1058–1068. [PubMed: 18404706]
20. Jere D, Jiang HL, Kim YK, Arote R, Choi YJ, Yun CH, Cho MH, Cho CS. Chitosan-graft-polyethylenimine for Akt1 siRNA delivery to lung cancer cells. International Journal of Pharmaceutics. 2009; 378:194–200. [PubMed: 19501140]
21. Jiang HL, Kwon JT, Kim YK, Kim EM, Arote R, Jeong HJ, Nah JW, Choi YJ, Akaike T, Cho MH, Cho CS. Galactosylated chitosan-graft-polyethylenimine as a gene carrier for hepatocyte targeting. Gene Therapy. 2007; 14:1389–1398. [PubMed: 17637795]
22. Jiang HL, Nagaoka M, Kim YK, Arote R, Jere D, Park IY, Akaike T, Cho CS. Gene delivery to stem cells by combination of chitosan-graft-polyethylenimine as a gene carrier and E-cadherin-IgG Fc as an extracellular matrix. Journal of Biomedical Nanotechnology. 2007; 3:377–383.
23. Zou P, Yu YK, Wang YA, Zhong YQ, Welton A, Galban C, Wang SM, Sun DX. Superparamagnetic Iron Oxide Nanotheranostics for Targeted Cancer Cell Imaging and pH-Dependent Intracellular Drug Release. Molecular Pharmaceutics. 2010; 7:1974–1984. [PubMed: 20845930]
24. Chen R, Yu HI, Jia ZY, Yao QL, Teng GJ. Efficient nano iron particle-labeling and noninvasive MR imaging of mouse bone marrow-derived endothelial progenitor cells. International Journal of Nanomedicine. 2011; 6:511–519. [PubMed: 21468354]
25. Kievit FM, Veiseh O, Bhattarai N, Fang C, Gunn JW, Lee D, Ellenbogen RG, Olson JM, Zhang MQ. PEI-PEG-Chitosan-Copolymer-Coated Iron Oxide Nanoparticles for Safe Gene Delivery: Synthesis, Complexation, and Transfection. Advanced Functional Materials. 2009; 19:2244–2251. [PubMed: 20160995]
26. Veiseh O, Kievit FM, Fang C, Mu N, Jana S, Leung MC, Mok H, Ellenbogen RG, Park JO, Zhang M. Chlorotoxin bound magnetic nanovector tailored for cancer cell targeting, imaging, and siRNA delivery. Biomaterials. 2010; 31
27. Chen G, Chen W, Wu Z, Yuan R, Li H, Gao J, Shuai X. MRI-visible polymeric vector bearing CD3 single chain antibody for gene delivery to T cells for immunosuppression. Biomaterials. 2009; 30:1962–1970. [PubMed: 19162315]
28. Nasongkla N, Bey E, Ren JM, Ai H, Khemtong C, Guthi JS, Chin SF, Sherry AD, Boothman DA, Gao JM. Multifunctional polymeric micelles as cancer-targeted, MRI-ultrasensitive drug delivery systems. Nano Letters. 2006; 6:2427–2430. [PubMed: 17090068]
29. Shuai XT, Ai H, Nasongkla N, Kim S, Gao JM. Micellar carriers based on block copolymers of poly(e-caprolactone) and poly(ethylene glycol) for doxorubicin delivery. Journal of Controlled Release. 2004; 98:415–426. [PubMed: 15312997]
30. Guthi JS, Yang SG, Huang G, Li SZ, Khemtong C, Kessinger CW, Peyton M, Minna JD, Brown KC, Gao JM. MRI-Visible Micellar Nanomedicine for Targeted Drug Delivery to Lung Cancer Cells. Molecular Pharmaceutics. 2010; 7:32–40. [PubMed: 19708690]
31. Hong GB, Yuan RX, Liang BL, Shen J, Yang XQ, Shuai XT. Folate functionalized polymeric micelle as hepatic carcinoma-targeted, MRI-ultrasensitive delivery system of antitumor drugs. Biomedical Microdevices. 2008; 10:693–700. [PubMed: 18350380]
32. Lucke A, Tessmar J, Schnell E, Schmeer G, Gopferich A. Biodegradable poly(D,L-lactic acid)-poly(ethylene glycol)-monomethyl ether diblock copolymers: structures and surface properties relevant to their use as biomaterials. Biomaterials. 2000; 21:2361–2370. [PubMed: 11055283]
33. Sun SH, Zeng H. Size-controlled synthesis of magnetite nanoparticies. Journal of the American Chemical Society. 2002; 124:8204–8205. [PubMed: 12105897]
34. Mykhaylyk O, Antequera YS, Vlaskou D, Plank C. Generation of magnetic nonviral gene transfer agents and magnetofection in vitro. Nature Protocols. 2007; 2:2391–2411.
35. Lee ES, Na K, Bae YH. Polymeric micelle for tumor pH and folate-mediated targeting. Journal of Controlled Release. 2003; 91:103–113. [PubMed: 12932642]
36. Cheng D, Hong GB, Wang WW, Yuan RX, Ai H, Shen J, Liang BL, Gao JM, Shuai XT. Nonclustered magnetite nanoparticle encapsulated biodegradable polymeric micelles with enhanced properties for in vivo tumor imaging. Journal of Materials Chemistry. 2011; 21:4796–4804.

37. Lai JR, Chang YW, Yen HC, Yuan NY, Liao MY, Hsu CY, Tsai JL, Lai PS. Multifunctional doxorubicin/superparamagnetic iron oxide-encapsulated Pluronic F127 micelles used for chemotherapy/magnetic resonance imaging. Journal of Applied Physics. 2010; 107
38. Jung CW, Jacobs P. Physical and chemical-properties of superparamagnetic iron-oxide MR contrast agents ferumoxides, ferumoxtran, ferumoxsil. magnetic resonance imaging. 1995; 13:661–674. [PubMed: 8569441]
39. Dutta P, Pai S, Seehra MS, Shah N, Huffman GP. Size dependence of magnetic parameters and surface disorder in magnetite nanoparticles. Journal of Applied Physics. 2009; 105
40. Dastan T, Turan K. In vitro characterization and delivery of chitosan-DNA microparticles into mammalian cells. Journal of Pharmacy and Pharmaceutical Sciences. 2004; 7:205–214. [PubMed: 15367377]
41. Jiang HL, Kwon JT, Kim EM, Kim YK, Arote R, Jere D, Jeong HJ, Jang MK, Nah JW, Xu CX, Park IK, Cho MH, Cho CS. Galactosylated poly(ethylene glycol)-chitosan-graft-polyethylenimine as a gene carrier for hepatocyte-targeting. Journal of Controlled Release. 2008; 131:150–157. [PubMed: 18706946]
42. Wong K, Sun GB, Zhang XQ, Dai H, Liu Y, He CB, Kw Leong. PEI-g-chitosan, a novel gene delivery system with transfection efficiency comparable to polyethylenimine in vitro and after liver administration in vivo. Bioconjugate Chemistry. 2006; 17:152–158. [PubMed: 16417264]
43. Chou LYT, Ming K, Chan WCW. Strategies for the intracellular delivery of nanoparticles. Chemical Society Reviews. 2011; 40:233–245. [PubMed: 20886124]
44. Duan H, Nie S. Cell-penetrating quantum dots based on multivalent and endosomolytic surface coatings. Abstracts of Papers of the American Chemical Society. 2007; 233
45. Wang YXJ, Hussain SM, Krestin GP. Superparamagnetic iron oxide contrast agents: physicochemical characteristics and applications in MR imaging. European Radiology. 2001; 11:2319–2331. [PubMed: 11702180]
46. Gao GH, Im GH, Kim MS, Lee JW, Yang J, Jeon H, Lee JH, Lee DS. Magnetite-Nanoparticle-Encapsulated pH-Responsive Polymeric Micelle as an MRI Probe for Detecting Acidic Pathologic Areas. Small. 2010; 6:1201–1204. [PubMed: 20449849]
47. Lee PW, Hsu SH, Wang JJ, Tsai JS, Lin KJ, Wey SP, Chen FR, Lai CH, Yen TC, Sung HW. The characteristics, biodistribution, magnetic resonance imaging and biodegradability of superparamagnetic core-shell nanoparticles. Biomaterials. 2010; 31:1316–1324. [PubMed: 19959224]
48. Thorek DLJ, Chen A, Czupryna J, Tsourkas A. Superparamagnetic iron oxide nanoparticle probes for molecular imaging. Annals of Biomedical Engineering. 2006; 34:23–38. [PubMed: 16496086]

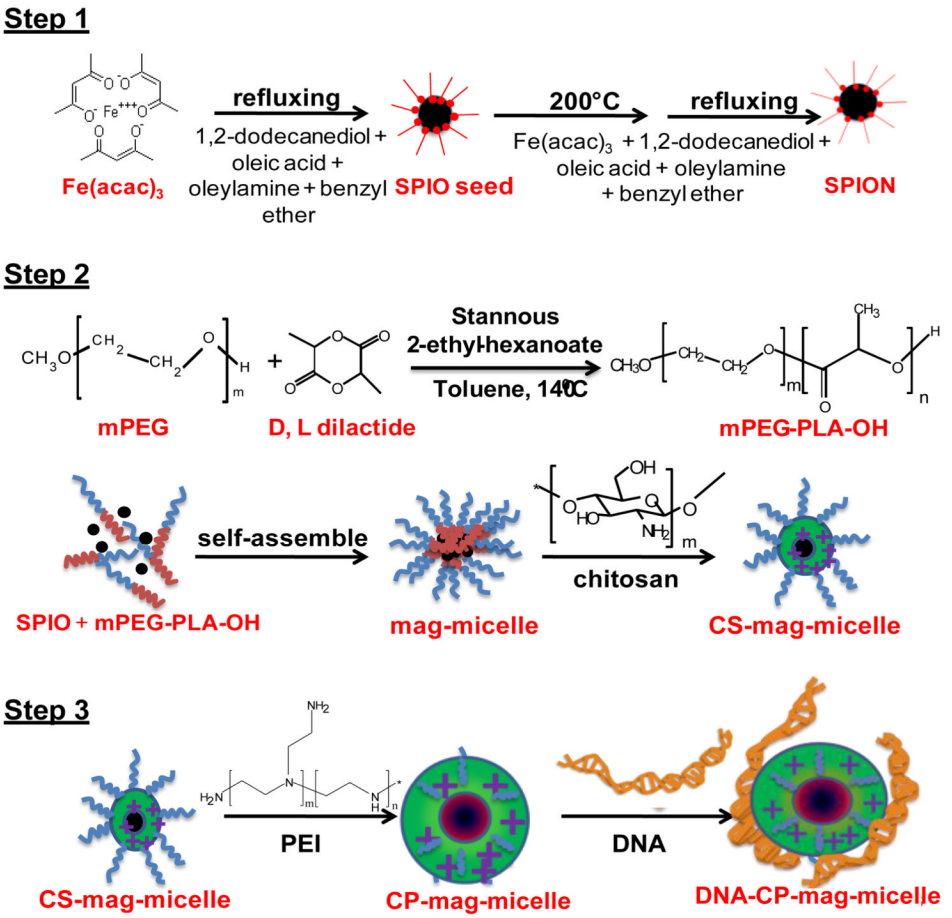

Figure 1.
Schematic illustration of the dual-purpose CP-mag-micelle synthesis.

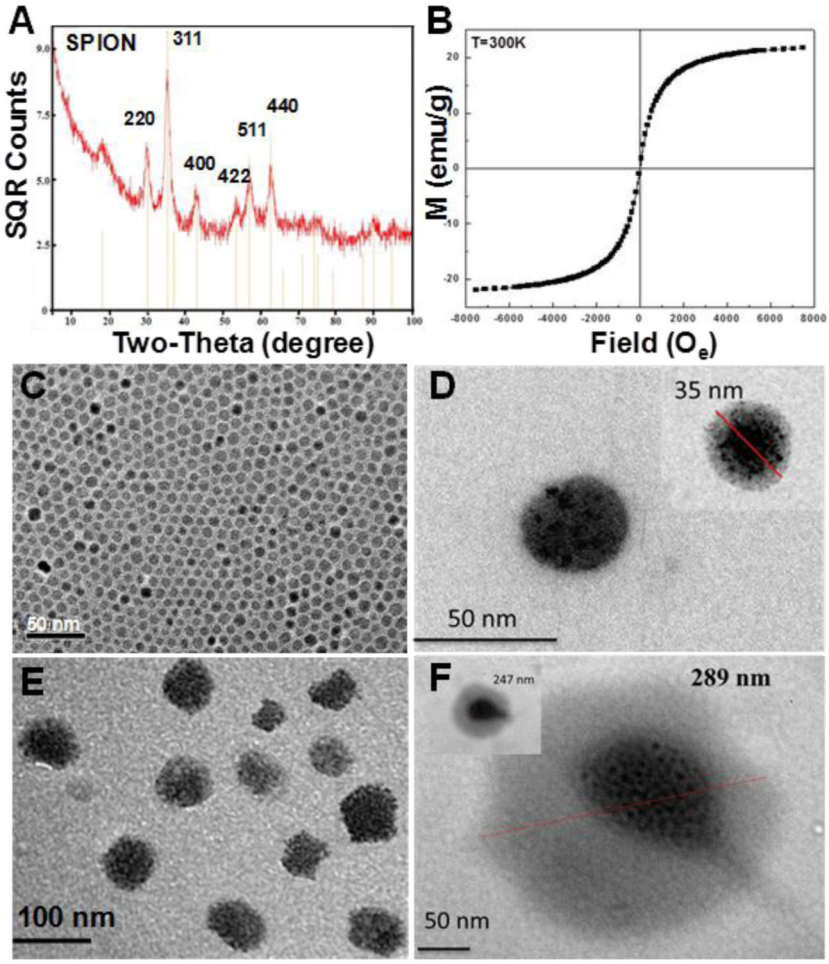

Figure 2.

XRD spectra of SPION (A), Magnetization vs. magnetic field of SPIONs 300K (B). TEM of SPIONs (C), mag-micelle (D), CP-mag-micelle (chitosan:PEI wt ratio, 5:5) (E), and CP-mag-micelle:DNA (wt ratio of chitosan:PEI:DNA, 5:5:1) (F).

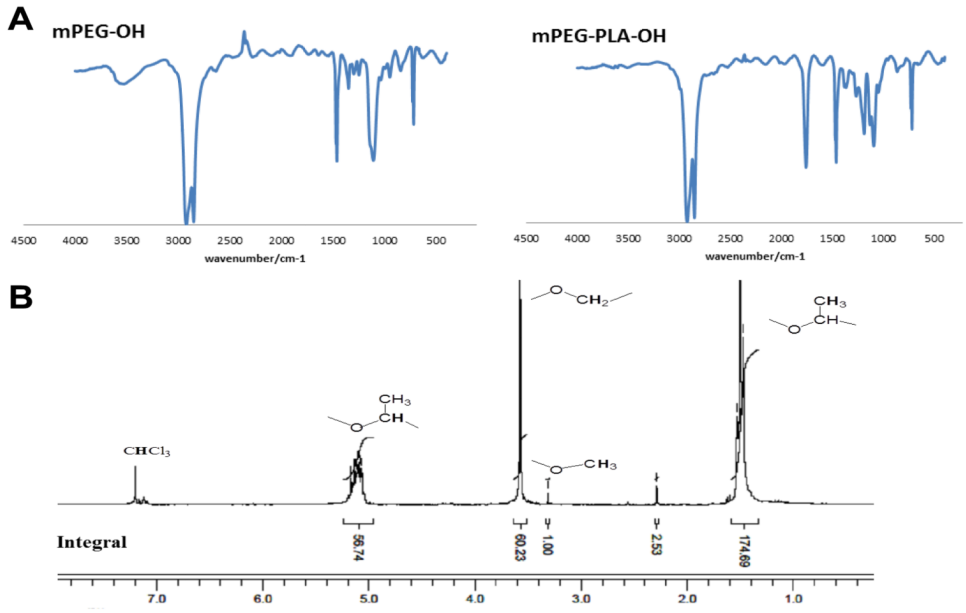

Figure 3.
FTIR spectrum of mPEG-OH and mPEG-PLA-OH (A) and NMR of mPEG-PLA (B).

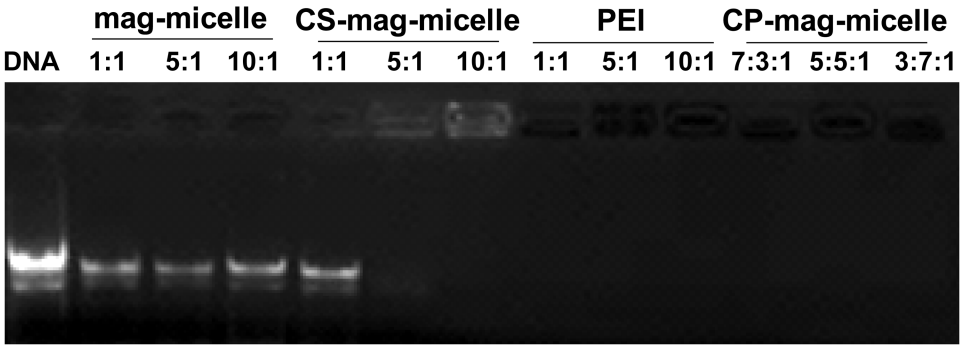

Figure 4.
Gel electrophoresis of the complexes of mag-micelles and DNA at different wt ratios, CS-mag-micelles and DNA at different wt ratios, PEI and DNA at different wt ratios, CP-mag-micelles and DNA with different chitosan:PEI:DNA wt ratios.

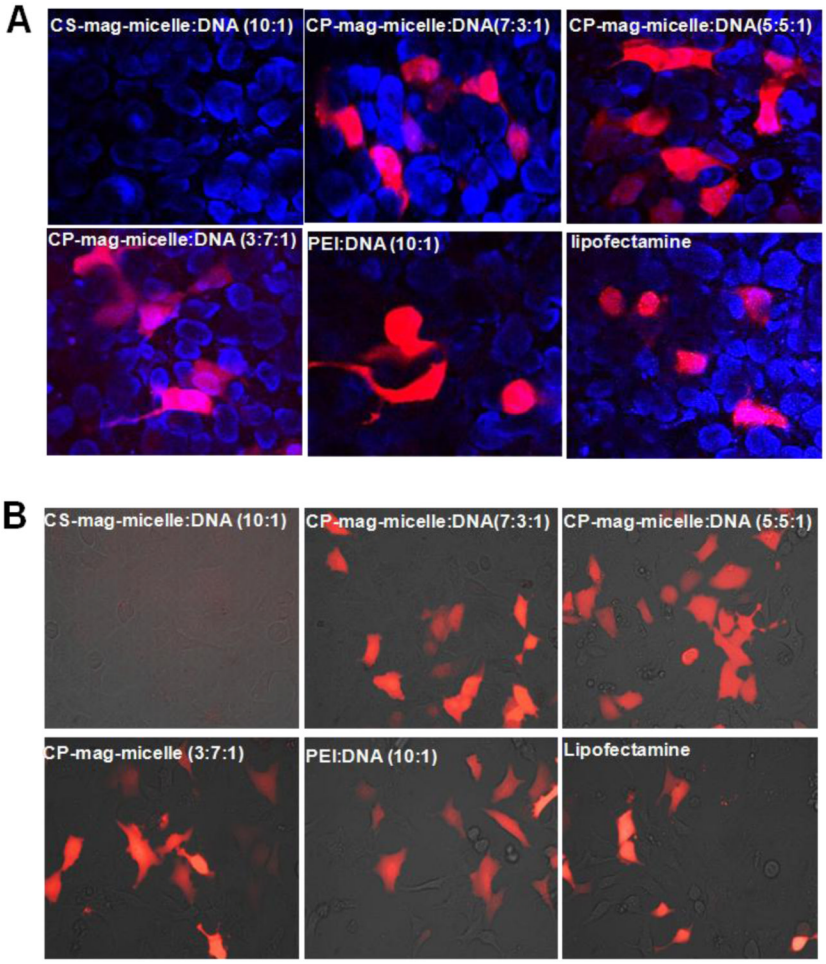

Figure 5.

Cells were transfected with indicated NPs complexed with Tomato red-fluorescent protein plasmid. Forty-eight hours after transfection, tomato protein expression was examined. Confocal microscopic images (200×) of HEK293. Nuclei were stained with DAPI (A). Fluorescence images (400×) of 3T3 cells (B).

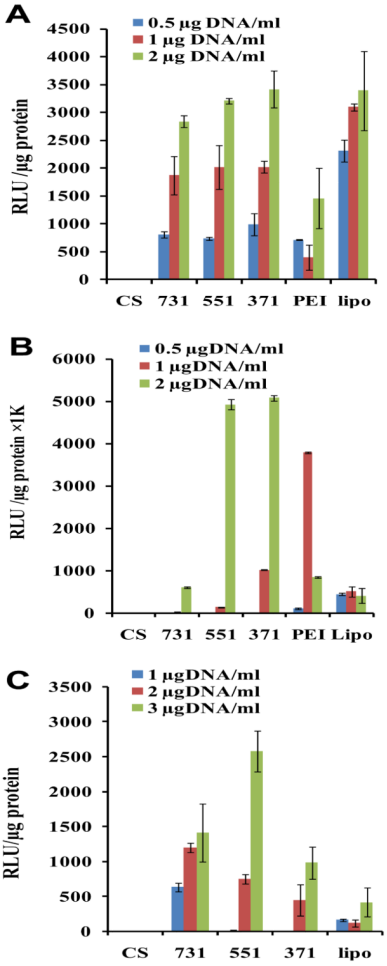

Figure 6.

Transfection efficiencies of HEK 293 cells (A), 3T3 cells (B) and PC3 cells (C) treated with either CS-mag-micelle:DNA (10:1) (CS),CP-mag-micelle:DNA complexes with varying wt ratios, chitosan:PEI:DNA (7:3:1), chitosan:PEI:DNA (5:5:1), chitosan:PEI:DNA (3:7:1), PEI:DNA (10:1) (PEI), and Lipofectamine (lipo).

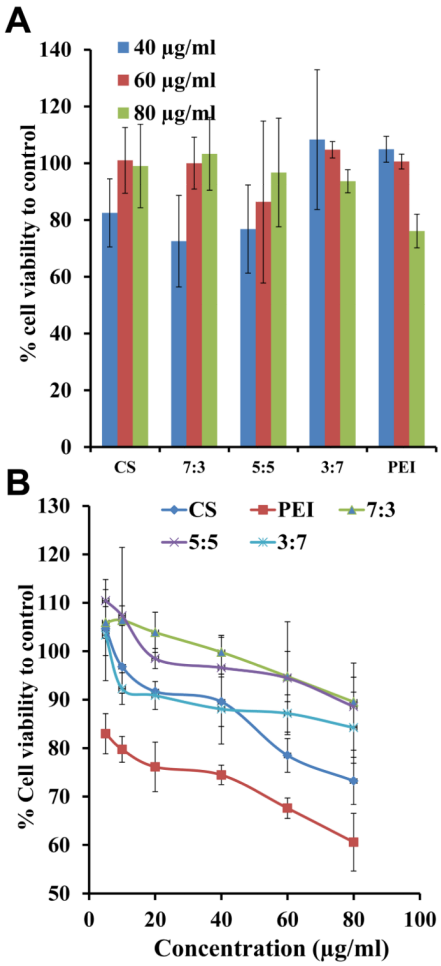

Figure 7.

Viability of PC3 (A) and HEK293 (B) cells treated with different concentrations of CS-mag-micelles, CP-mag-micelles (7:3), CP-mag-micelles (5:5), CP-mag-micelles (3:7) and PEI.

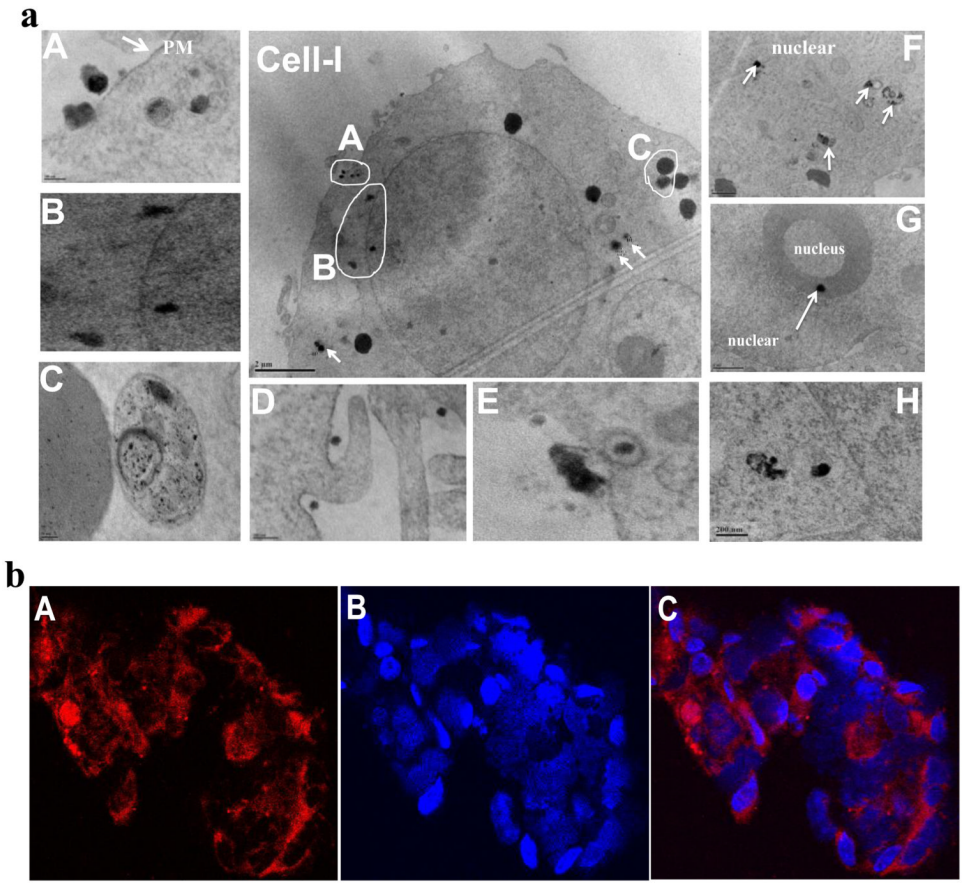

Figure 8.

(a) TEM images showing uptake and intracellular distribution of CP-mag-micelle:DNA (wt ratio of chitosan:PEI:DNA, 5:5:1) by PC3 cells. A-C images are expanded from Cell-I. (b) Laser confocal microscopic images (600×) of HEK293 cells incubated with Cy5.5-CP-mag-micelles (wt ratio of chitosan:PEI, 5:5) for 3 h: Cy5.5(A), DAPI(B), overlay(C).

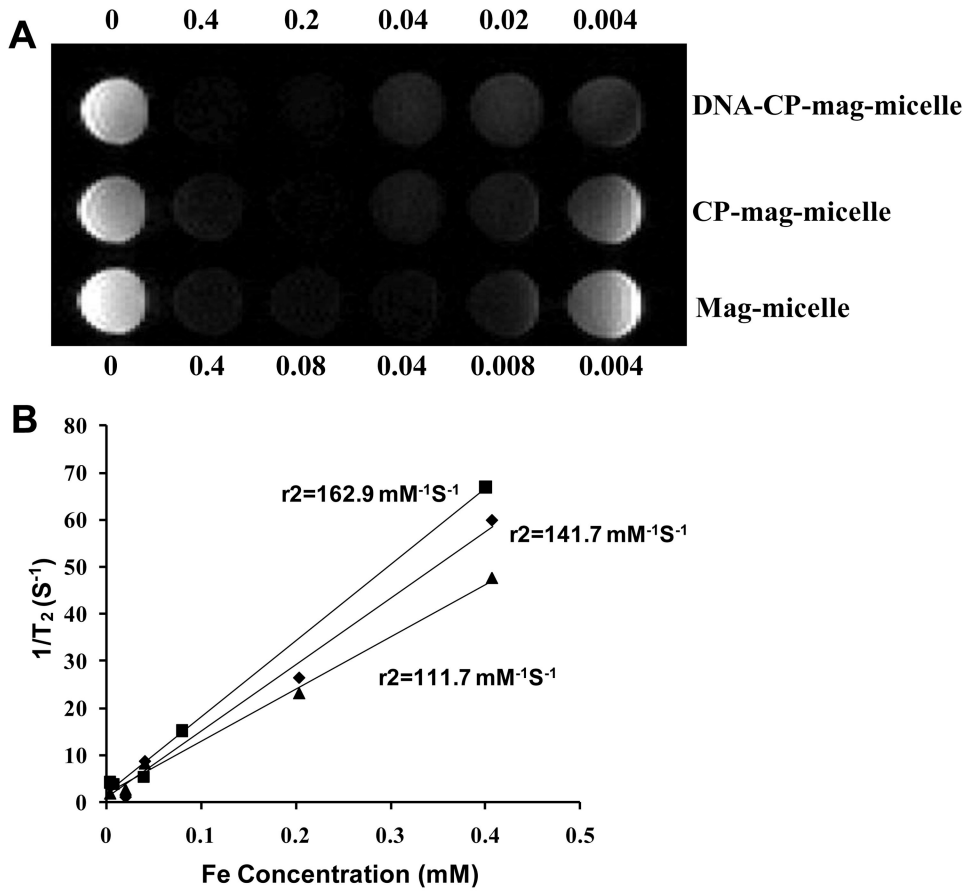

Figure 9.

Magnetic properties of NPs: (A) T2-weighted MRI-images of mag-micelles, CP-mag-micelles (chitosan:PEI wt ratio, 5:5) and CP-mag-micelle:DNA (wt ratio of chitosan:PEI:DNA, 5:5:1) (B) corresponding r_2 values of mag-micelles (■),CP-mag-micelles (◆),CP-mag-micelle:DNA (▲).

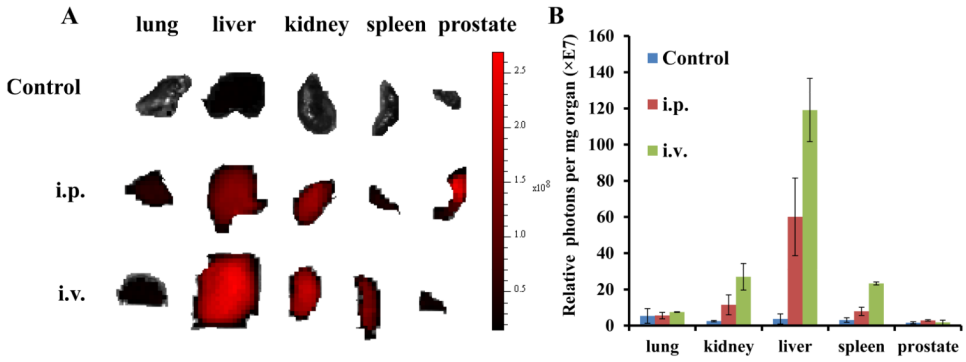

Figure 10.

Biodistribution of Cy5.5-conjugated CP-mag-micelles in mice by Xenogen imaging. (A) Mice were given PBS (control) or Cy5.5-CP-mag-micelles (1μg/μl, 500μl) by i.p (n=2) or i.v. Cy5.5-CP-mag-micelle (5μg/μl, 100μl) (n=2). Four hours after administration, fluorescence images of whole organs were acquired using the Xenogen imaging system. The spectrum gradient bar corresponds to the fluorescence intensity unit p/sec/cm2/sr. Since PBS treated mice (i.p. and i.v.) showed little fluorescence intensity, only representative sections from one of the PBS treated mice are shown. B) Relative photon intensity per mg organ weight is shown.

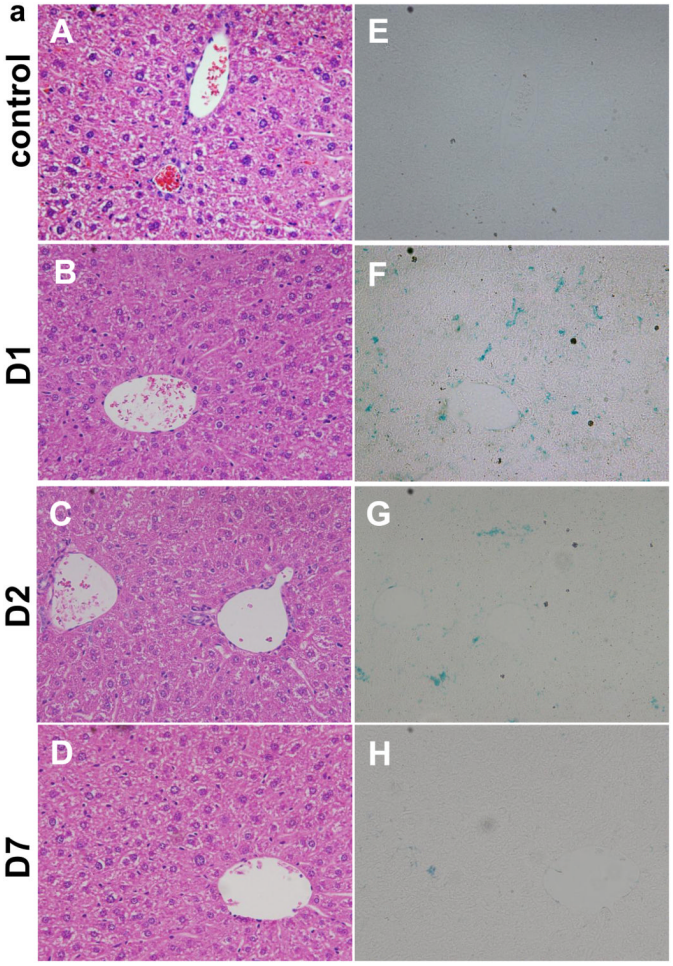

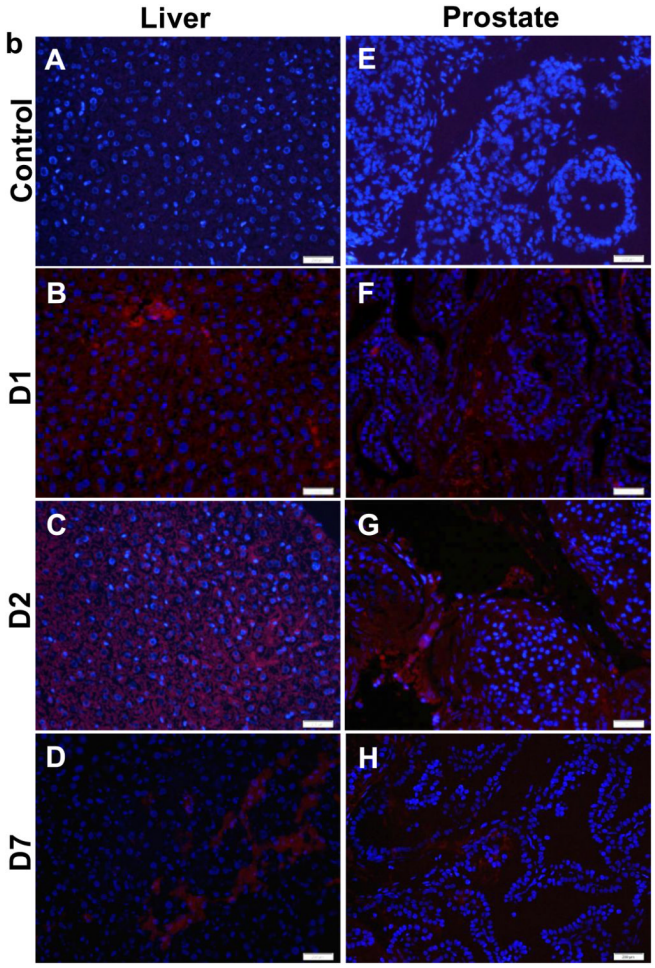

Figure 11.

(a) H&E staining of paraffin-fixed liver tissues: control (A), one day (D1, B), two days (D2, C), seven days (D7, C). Prussian blue staining of fixed paraffin-embedded liver tissues: control (E), one day (D1, F), two days (D2, G), seven days (D7, H). (b) in vivo gene transfection of liver with control (A) at one day (D1, B), two days (D2, C) and seven days (D7, D); in vivo gene transfection of prostate with control (E) at one day (D1, F), two days (D2, G) and seven days (D7, H)